Nat Med. Author manuscript; available in PMC 2015 June 01.

Published in final edited form as:
Nat Med. 2014 December ; 20(12): 1458–1463. doi:10.1038/nm.3709.

Immune complexes stimulate CCR7-dependent dendritic cell migration to lymph nodes

Menna R. Clatworthy[1,2,3], **Caren E. Petrie Aronin**[2], **Rebeccah J. Mathews**[1], **Nicole Morgan**[4], **Kenneth G.C. Smith**[5], and **Ronald N. Germain**[2,3]

[1]University of Cambridge Department of Medicine, Laboratory of Molecular Biology, Francis Crick Avenue, Cambridge Biomedical Campus, Cambridge, CB2 0QH. UK

[2]Laboratory of Systems Biology (LSB), Lymphocyte Biology Section (LBS), National Institute of Allergy and Infectious Diseases, National Institutes of Health, Bethesda, MD, 20892-1892, USA

[4]Biomedical Engineering and Physical Sciences Resource (BEPS), Microfabrication and Microfluidics Unit (MMU), National Institute of Biomedical Imaging and Bioengineering, National Institutes of Health, Bethesda, MD, 20892-1892, USA

[5]Cambridge Institute for Medical Research and Department of Medicine, University of Cambridge School of Clinical Medicine, Cambridge, CB2 0XY. UK

Abstract

Antibodies are critical for defence against a variety of microbes but may also be pathogenic in some autoimmune diseases. Many effector functions of antibody are mediated by Fcγ receptors (FcγRs), which are found on most immune cells, including dendritic cells (DCs). DCs are important antigen presenting cells and play a central role in inducing antigen-specific tolerance or immunity[1,2]. Following antigen acquisition in peripheral tissues, DCs migrate to draining lymph nodes via lymphatics to present antigen to T cells. In this study we demonstrate that FcγR engagement by IgG immune complexes (IC) stimulates DC migration from peripheral tissues to the paracortex of draining lymph nodes. *In vitro*, IC-stimulated murine and human DCs showed enhanced directional migration in a CCL19 gradient and increased CCR7 expression. Using intravital two-photon microscopy, we observed that local administration of IC resulted in dermal DC mobilisation. We confirmed that dermal DC migration to lymph nodes was CCR7-dependent and increased in the absence of the inhibitory receptor, FcγRIIb. These observations have relevance to autoimmunity, because autoantibody-containing serum from mice and humans with SLE also increased dermal DC migration to lymph nodes *in vivo*, suggesting that this process may occur in lupus, potentially driving the inappropriate localisation of autoantigen-bearing DCs.

[3]**Corresponding authors contact: Menna R. Clatworthy** BSc, MBBCh, FRCP, PhD, University of Cambridge Research Unit, MRC Laboratory of Molecular Biology, Cambridge Biomedical Campus, Cambridge. CB2 0QH, UK, Phone: 44 1223 267279, Fax: 44 1223 268303, mrc38@cam.ac.uk; **Ronald N. Germain** MD, PhD, Bldg. 4, Rm. 126A, National Institutes of Health, Bethesda, MD 20892, USA, Phone: 01 301-496-1904, Fax: 01 301-480-1660, rgermain@nih.gov.

Author Contributions

MRC conceived the project, carried out experiments, designed and supervised experiments, analysed data and wrote the manuscript. CEPA and RJM carried out experiments and analysed data. NM provided technical advice to CEPA for the *in vitro* DC chemotaxis assay. KGCS provided mentorship for MRC and scientific advice. RNG provided advice on experimental design, assisted with manuscript writing and editing and provided mentorship for MRC and CEPA.

Europe PMC Funders Author Manuscripts

Antibodies have direct protective effects via pathogen or toxin neutralisation and can activate complement or ligate Fc receptors[3,4]. FcγR bind immune complexed IgG and include activating receptors (in humans FcγRIIA, IIIA and IIIB) and a single inhibitory receptor FcγRIIB[5]. DCs express a number of receptors, among them FcγRs, which allow antigen internalisation for processing and presentation to T cells[1,2,6]. Recognition of this displayed antigen may induce T cell tolerance or activation, a cellular decision influenced by the provision of co-stimulatory signals present on mature, but not on immature DCs[7,8]. DC maturation may be driven by a variety of stimuli, including TLR ligands, pro-inflammatory cytokines, and by activating FcγR cross-linking[9,10]. The inhibitory receptor FcγRIIB provides a basal level of inhibition to DC maturation in the presence of ICs, thereby regulating immunogenic antigen presentation to T cells and providing an important tolerance checkpoint[11-15]. A number of stimuli preferentially reduce FcγRIIB expression on monocytes, notably interferon-γ (IFN-γ)[16], allowing these cells to be activated and matured by subsequent encounter with IC. Deficiency or dysfunction of FcγRIIB is associated with the IC-mediated autoimmune disease systemic lupus erythematosus (SLE) in both mice and humans[17-22].

In addition to a requirement for maturation, tissue resident DCs must be geographically re-located from peripheral tissues to lymph nodes to permit interactions with T cells[23, 24-26]. Studies to date on the role of FcγRs in DCs have focused on the effects of antibody and FcγR-crosslinking on DC maturation but none have addressed the crucial question of how antibody engagement of FcγRs might affect the migration and anatomical repositioning of DCs.

To determine if FcγR cross-linking with IC might alter DC migration from peripheral tissue to lymph nodes, we stimulated bone marrow-derived DCs with ovalbumin (OVA) or IgG-opsonised OVA (IC) for 24 hours, and subsequently transferred the DCs subcutaneously to a recipient mouse. Draining lymph nodes were harvested 48 hours following DC transfer and migration assessed by histological quantification. Following exposure to OVA alone, a limited number of wild type (WT) DCs were observed, whereas a substantially greater number of IC-stimulated WT DCs were present within the lymph node paracortex (Fig.1a). We next used FcγRIIb-deficient DCs to model the effect of administering IC to activated DCs (on which FcγRIIb is down-regulated[11-13]) or DCs from individuals with dysfunctional FcγRIIb[21]. Forty-eight hours following DC transfer, the number of IC-stimulated *Fcgr2b*$^{-/-}$ DCs observed in the lymph node paracortex was significantly higher than the number of IC-stimulated WT DCs (Fig. 1a-c). To control for variations in DC administration and local tissue anatomy, we also co-transferred WT and FcγRIIb-deficient DCs into a single site. These experiments confirmed increased migration of IC-stimulated *Fcgr2b*$^{-/-}$ DCs to lymph nodes (Fig. 1d,e), as did lymph node disruption and DC enumeration by flow cytometry (Fig. 1f). We verified the viability of migrating DC by intravital imaging of lymph nodes (Supplementary Video 1) and by flow cytometry (Supplementary Fig. 1).

To dissect the mechanisms underpinning IC-induced DC migration, we considered a variety of factors known to affect this process. In particular, DCs express the chemokine receptor CCR7, which interacts with CCL19 and CCL21 expressed on lymphatics[25,26]. IC

stimulation resulted in a modest upregulation of CCR7 expression on WT DCs but a significant upregulation on FcγRIIb-deficient DCs (Fig. 1g). A second factor we considered was the production of matrix metalloproteinases (MMPs), since migrating DCs secrete MMPs, particularly MMP-2 and MMP-9[27,28], to facilitate movement through the extracellular matrix and across basement membranes. Pharmacological inhibition[29], antibody neutralization[30], or genetic deletion of MMPs[27,28,31] reduces DC migration. *In vitro*, within 4 hours of FcγR-cross-linking, WT DCs produced proteases capable of gelatin digestion (Fig. 1h, Supplementary Fig. 2). This response was increased in FcγRIIb-deficient DCs (Fig. 1h), as were levels of MMP-9 in DC culture supernatants (Fig. 1i). IC-induced MMP-9 production by murine DCs was abrogated by ERK inhibition, but not by JNK or p38 inhibition (Supplementary Fig. 3).

To further explore the possible role of IC-induced upregulation of CCR7 on DC chemotaxis, we used a three dimensional *in vitro* model, embedding IC-stimulated DCs within a collagen matrix (Fig. 2a) in a rising soluble CCL19 gradient (Petrie Aronin *et al.* 2014, manuscript in preparation). IC-stimulated WT DCs showed increased migration towards CCL19 compared with OVA-stimulated DCs (Fig. 2b-d, Supplementary Fig. 4, Supplementary Videos 2, 3). In the absence of FcγRIIb, IC-stimulated DCs showed even greater directional migration (Fig. 2b-d, Supplementary Fig. 4, Supplementary Videos 4, 5). The capacity of IC to stimulate DC chemotaxis was FcγRIII-dependent (Fig. 2e, Supplementary Fig. 5a), as was IC-mediated upregulation of CCR7 and MMP9 (Supplementary Fig. 5b, c). CCR7-deficiency abrogated IC-induced DC migration to draining lymph nodes following subcutaneous transfer (Fig. 2f, Supplementary Fig. 6).

To determine the relevance to human DCs, we generated DCs from peripheral blood monocytes obtained from healthy donors. These DCs demonstrated a significant increase in CCR7 expression post-stimulation with ICs (Fig. 2g) and there was an increase in their directional migration in a CCL19 gradient (Fig. 2h-i, Supplementary Videos 6, 7) and in MMP-9 production (Fig. 2j).

Given our quantitative migration data in the DC transfer model and the *in vitro* data, we wished to determine if the administration of ICs was sufficient to stimulate endogenous DC migration *in vivo*. Utilising intravital two-photon microscopy to assess the dynamic behaviour of dermal DCs in CD11cEYFP mice, we found that administration of IC into the footpad resulted in mobilisation of these cells (consistent with chemotaxis or chemokinesis), as compared with injection of OVA alone (Fig. 3a, b and Supplementary Videos 8, 9). These cells did not express granulocyte or monocyte markers (Supplementary Fig. 7) and were observed clustering around, entering into, and travelling within lymphatic vessels following IC stimulation (Fig. 3c, Supplementary Video 10, Supplementary Figs. 8, 9). IC-induced dermal DC mobilisation was even greater in *Fcgr2b*$^{-/-}$ CD11cEYFP mice (Fig. 3a,b and Supplementary Videos 11, 12) supporting the idea that human subjects with FcγRIIb dysfunction might demonstrate increased IC-induced DC motility.

Intravital imaging of skin DCs only allows the visualisation of the initial phase of DC migration, therefore, we sought to determine if IC-stimulated dermal DCs complete their journey to draining lymph nodes. FITC-painting was used to label dermal DCs, followed by

local administration of OVA or IC. In WT mice, a significantly greater number of FITC^{+}/MHC class II^{high}/CD11c^{+} cells were present in draining lymph nodes following IC stimulation compared with OVA stimulation (Fig. 3d,e) and these cells expressed markers typical of skin-resident, migratory DCs (Fig. 3d). A significantly greater accumulation of FITC-labelled DCs was observed in *Fcgr2b*$^{-/-}$ mice following IC stimulation (Fig. 3 d,e). CCR7-deficient dermal DCs showed severely impaired migration to draining lymph nodes in response to IC stimulation (Fig. 3f,g, Supplementary Fig. 10). MMP-9 blockade had a less potent effect on IC-mediated dermal DC migration (Fig. 3h, Supplementary Fig. 11).

Since local administration of IC induced DC migration *in vivo*, we hypothesised that this phenomenon would have relevance to SLE, a disease characterised by IC deposition in tissues, including skin[32]. Of note, abnormalities in monocytes and DCs have been observed in patients with lupus[33,34,35,36]. To address the question of whether lupus ICs might stimulate DC mobilisation *in vivo* we injected heat-inactivated serum, taken from either NZB/W F1 mice with anti-nuclear antibodies and nephritis (a mouse model of human SLE) or aged-matched controls, into the footpads of CD11cEYFP mice. NZB/W F1 serum stimulated dermal DC mobilisation (Fig. 4a,b, Supplementary Video 13), in contrast to footpads treated with control serum (Figure 4 a,b, Supplementary Video 14, Supplementary Fig 12a,b). The stimulatory effect of lupus serum on dermal DC motility was IgG-dependent (Fig. 4c, Supplementary Fig. 12c). We also observed an increased number of FITC-labelled dermal DCs in the draining lymph nodes of mice to which lupus serum had been transferred intraperitoneally, compared with those that received WT serum (Fig. 4d,e). In addition, in renal draining lymph nodes of aged NZM mice with lupus nephritis, the number of migratory DCs (CD11c^{+}/MHCII^{high}/CD103^{+}) was significantly greater than that observed in aged-match NZW controls, in which such cells were scarcely detectable (Fig. 4f, Supplementary Fig. 13).

To explore the relevance of these observations to human disease, we administered heat-inactivated serum from human patients with lupus into the footpads of CD11cEYFP mice. This resulted in increased dermal DC migration compared with healthy control serum, particularly when the serum was obtained from patients with high disease activity scores (Fig. 4g,h, Supplementary Fig. 14, Supplementary Videos 15,16). In addition, we examined the effect of a polymorphism in human *FCGR2B* (rs1050501) on DC CCR7 expression. This polymorphism involves an amino acid substitution in the transmembrane domain, a threonine replacing an isoleucine (FcγRIIB-T232), resulting in receptor dysfunction[21,22], and contributing to lupus susceptibility[37]. U937 cells stably transfected with FcγRIIB-I232 or FcγRIIBT232[21] were differentiated to a DC phenotype, and stimulated with IC. IC-dependent CCR7 expression was significantly higher on cells transfected with the dysfunctional FcγRIIBT232 compared with those transfected with FcγRIIBI232 (Fig. 4i), suggesting that DCs from individuals with the lupus-associated polymorphism would show increased migration when exposed to ICs, analogous to our observations in *Fcgr2b*$^{-/-}$ mice.

In conclusion, our study demonstrates a novel effect of antibody-opsonisation, namely increased DC migration to lymph nodes via FcγR-induced upregulation of CCR7 and MMPs. This would allow the optimal positioning of DCs in the lymph node paracortex, acting synergistically with the known effects of activating FcγR-cross-linking on class II and

Europe PMC Funders Author Manuscripts

co-stimulatory molecule upregulation on these cells, to promote immunogenic T cell-DC interactions. Furthermore, we show that dermal DC migration is increased following administration of ICs or autoantibody-containing serum, and this effect is particularly pronounced in the absence of the inhibitory receptor FcγRIIb, a known susceptibility locus in SLE. Together, these data suggest an additional mechanism by which ICs might drive autoimmunity in SLE via the inappropriate localisation of autoantigen-bearing DC and may also have implications for boost strategies in vaccination.

Supplementary methods

Mice

FcγRIIb-deficient mice on a C57BL/6 background[18] were kindly provided by Jeff Ravetch (Rockefeller University, New York) and Silvia Bolland (National Institutes of Health, NIAID, Bethesda, MD) and crossed to transgenic mice expressing EGFP under the control of the human ubiquitin C promoter[38] (Jackson Laboratories) or transgenic mice expressing Venus EYFP under the control of the CD11c promoter[39] (obtained from M. Nussenzweig, Rockefeller University, New York, NY). C57BL/6 mice were obtained from Jackson Laboratories or from Charles River Laboratories (Margate, UK). NZB/W F1 were bred in-house from NZB and NZW mice obtained from Harlan UK. CCR7-deficient mice on a C57BL/6 background (strain B6.129P2(C)-Ccr7^{tm1Rfor}/J, stock number 006621, live repository, aged 8 weeks old) were purchased from Jackson Laboratories. Age matched C57BL/6 JAX mice were used as controls. In all experiments, both male and female mice were used. Mice were maintained in specific-pathogen-free conditions at an Association for Assessment and Accreditation of Laboratory Animal Care-accredited animal facility at NIAID or at a Home Office-approved facility in the UK. All procedures were approved by the NIAID Animal Care and Use Committee (National Institutes of Health, Bethesda, MD) or were conducted in accordance with the United Kingdom Animals (Scientific Procedures) Act 1986.

Antibodies

For immunofluorescence and flow cytometric studies, the following antibodies were used;

For immunofluorescence and flow cytometric studies, the following antibodies were used. For each antibody the clone and the product code (catalogue number) are provided;

Murine antibodies: anti-B220 antibody (clone RA3-6B2, product code 561877), anti-CD3 antibody (clone 17A2, 561389) (BD Biosciences, San Jose, CA), PE-conjugated anti-mouse CCR7 (clone 4B12, 12-1971), PeCy7-conjugated anti-CD4 (clone RM4-5, 25-0042), PeCy7-conjugated anti-CD19 (clone eBio 1D3, 25-0193), FITC-conjugated anti-CD11b (clone M1/70, 53-0112) Alexa Fluor 780-conjugated CD11c (clone N418, 47-0114), Pacific Blue-conjugated anti-class II (clone AF6-120.1, 48-5320), PE-conjugated anti-CD103 (clone 2E7, 12-1031), APC-conjugated anti-EpCAM (clone G8.8, 17-5791), ef450-conjugated Gr-1 (clone RB6-8C5), and PE-conjugated Ly6C (Clone HK1.4).

Human antibodies: PE-Cy7-conjugated anti-CCR7 (clone 3D12, 560922, BD Pharmingen, San Diego, CA), PE-Cy7- conjugated Rat IgG2a isotype control (557855, BD Pharmingen),

APC- conjugated CD86 (clone 2331, 560956), FITC-conjugated HLA DR (clone G46-6, 560944, BD Pharmingen).

All antibodies were obtained from eBioscience (San Diego, CA), unless otherwise indicated, and used at 1/200 dilution, (except for the MHC class II antibody, which was used at 1/100). For some flow cytometric studies, a Live/Dead Fixable Aqua Dead Cell Stain Kit (Invitrogen-Molecular Probes, Carlsbad, CA) was used.

Immune complexes

Endotoxin-free ovalbumin (EndoGrade Ovalbumin, Hyglos GmbH) was opsonised with a polyclonal rabbit anti-ovalbumin antibody (Sigma-Aldrich, St. Louis, MO) at 37 °C for 1 hour.

DC culture and stimulation

We generated primary murine bone marrow-derived DCs as described previously[40]. Briefly, bone marrow was flushed from femurs and tibias, plated in regular petri dishes at 2.5×10^6 cells per dish, and supplemented with 20 ng ml^{-1} granulocyte-macrophage colony-stimulating factor (GM-CSF, Peprotech Rocky Hill, NJ) in base media (10% Hyclone FBS, 1% penicillin/streptomycin in RPMI 1640) 3 times over 8 days. On Day 9, DCs were transferred to tissue culture plates and incubated overnight with endotoxin-free ovalbumin (EndoGrade Ovalbumin, Hyglos GmbH, Starnberger, Germany) or immune-complexed ovalbumin for 24 hours at 37 °C.

We generated human monocyte-derived DCs from the peripheral blood of healthy volunteers. Samples were obtained with informed consent and the approval of the Cambridge Local Research Ethical committee (reference 08/H0308/176) or from normal volunteers from the NIH Blood Bank. Blood was subjected to Ficoll–Hypaque density separation to isolate peripheral blood mononuclear cells and monocytes were enriched by negative selection by using a MACs-based monocyte purification kit (Miltenyi Biotec, Auburn, CA). DCs were generated by culturing the monocytes for 6 days with human GM-CSF (100 ng ml^{-1}, PeproTech) in DMEM supplemented with 10% heat-inactivated calf serum.

For murine FcγR blocking studies, anti-mouse FcγRIII (CD16, AF1960) or goat anti-mouse isotype control (AB-108-C both obtained from R&D Systems, Minneapolis, MN) were added to cells 1 hour prior to stimulation with IC (final concentration 1.5 μg ml^{-1}). Similarly, the PI3K inhibitor (ZSTK474, Selleckchem, 100 nM) or Akt inhibitor (AKT-XI (3-Formylchromone thiosemicarbazone, Cu(II)Cl_2 Complex, FPA-124), Merck-Millipore, 2.5 μM) was added to DCs prior to addition of IC and cells and supernatants harvested at 24 hours.

Cell lines

U937 cells stably transfected with vectors containing various isoforms of FcγRIIB (as described previously[21]) were utilized. Cells were cultured in RPMI 1640 with 10% FCS (Sigma) and penicillin/streptomycin (Sigma).

In vivo DC migration

24 hours following culture with ovalbumin or immune-complexed ovalbumin, 5×10^6 bone marrow derived DCs were washed in PBS to remove non-internalised ovalbumin or immune complexes, and injected subcutaneously in the flank or footpad (depending on the lymph node harvested). 48 hours following transfer, lymph nodes were harvested and processed for histological examination or flow cytometric analysis. Cells were labelled with Cell Tracker Orange (Invitrogen Molecular Probes) or Cell tracker Green (Invitrogen Molecular Probes) as indicated in figure legends.

Immunofluorescence microscopy

For quantification of DC migration to lymph nodes, lymph nodes were harvested and incubated in 0.05 M phosphate buffer containing 0.1 M L-lysine, pH 7.4, 2 mg mL^{-1} $NaIO_4$, and 10 mg mL^{-1} paraformaldehyde. Twelve hours later, lymph nodes were washed in phosphate buffer and dehydrated in 30% sucrose in phosphate buffer. Tissues were snap frozen in Tissue-Tek (Sakura Finetek, Netherlands). Frozen sections (50 μm) were stained with the indicated antibodies. Confocal images of whole lymph nodes sections were obtained using the tiling function of a Zeiss 710 or 780 microscope.

Flow cytometry

Cells were stained with the antibodies described above for 1 hour at 4 °C, with the exception of CCR7 staining, which was performed at room temperature. Samples were analysed using an LSR2 flow cytometer (Becton Dickinson, Basel, Switzerland). Data were processed using FlowJo software (Treestar, Ashland, TN).

MMP-9 measurement

Culture supernatants were obtained from bone marrow-derived dendritic cells after stimulation with OVA or IC, as indicated in the figure legends. Total MMP-9 was measured by ELISA (Duo Set, R&D Systems) according to manufacturer's instructions.

Matrix degradation

Glass coverslips were coated with 10 μg ml^{-1} FITC-gelatin (Invitrogen) and cross-linked with 0.5% glutaraldehyde [41]. 2×10^5 DC were plated onto matrix-coated coverslips and incubated at 37°C to allow degradation, then fixed with 4% paraformaldehyde (MP-Biomedicals) in phosphate buffered saline and stained with TRITC-phalloidin (Sigma) to outline the cell area. Matrix degradation and cell area were quantitated using Imaris software and the ratio calculated.

In Vitro Migration assay

The microfluidic-based migration chamber was fabricated utilizing methods established by Haessler *et al.*[42]. Briefly, source, sink and cell channels were patterned using commercial film masks generated by high-resolution laser photoplotting (CAD/Art Services, Bandon OR). Melted 3% agarose was poured onto the mask to create the desired channel pattern. These agarose stamps were incubated in 10% FBS with media for 24 hours. Device assembly included laying agarose stamps, channel side down, onto a glass coverslip. A

PMMA manifold containing inlet and outlet ports was placed on top of the agarose stamp, and the entire device was secured together with a metal clamp. EGFP DCs were mixed with Purecol bovine collagen I (final concentration 1.7mg/ml, Advanced Biomatrix, San Diego, CA) and loaded into the central channel. The chamber was incubated for 15 minutes at 37 °C, inverting once to ensure uniform cell distribution during collagen gelatination. Following incubation, a rising concentration of CCL19 (maximum concentration 100 ng mL^{-1}) (Peprotech, Rocky Hill, NJ) was applied to the source channel at 5 μL min^{-1}. The sink channel maintained base media under constant flow at 5 μL min^{-1}. Migratory behaviour was imaged on an inverted Zeiss 510 microscope under confocal settings with a 20 × 0.9 NA objective.

Intravital imaging of dermal DCs by two photon microscopy

CD11cEYFP mice were anaesthetised and Qdots A655 (Invitrogen Molecular Probes) administered intravenously to delineate dermal vasculature. Alternatively, rat anti-mouse LYVE-1 (clone 223322; R&D Systems) was covalently conjugated to HiLyte Fluor 594 using labeling kits (AnaSpec, Fremont, CA) and was administered into the footpad an hour prior to imaging. Footpad dermal DCs were imaged at 915nm using a Zeiss 510 microscope, as described previously[43,44]. To create a time-lapse sequence, a 70 μm-thick section of the dermis containing lymphatic vessels was scanned at 3 μm Z-steps every 50 seconds for an hour and 20 minutes, Imaging alternated between left and right footpads over an 8 hour period comparing footpads into which 50 μl of OVA or IC or heat inactivated serum had been injected 16 hours previously. OVA was placed into the right footpad and IC into the left footpad or control serum placed in left footpad and lupus serum placed in right footpad, allowing animals to act as their own controls. The investigator performing the imaging was not blinded to this information. The sample size for each experimental group included at least 3 mice, based on previous imaging studies performed in our laboratory this provides data on >50 DCs.

Mouse serum for in vivo studies

Serum was obtained from NZB/W F1 mice with anti-nuclear antibodies and nephritis (as evidenced by heavy proteinuria) and aged matched WT (C57BL/6) mice. Heat-inactivation was performed at 56 °C for 1 hour prior to administration. Some lupus sera were depleted of IgG using Nab Protein G spin columns (Thermo Scientific, Waltham, MA) following the manufacturers standard protocol.

FITC sensitisation dermal DC migration assay

FITC sensitisation was used to assess dermal DC migration, as described by Robbiani *et al.* [45]. Ovalbumin or immune-complexed ovalbumin was administered subcutaneously to the base of the tail, the flank or the groin on the right and left side respectively of C57BL/6 mice. This allows comparison of the two experimental conditions within the same animal. FITC (8 mg ml^{-1}, Sigma) was dissolved in equal volumes of acetone and dibutyl phthalate (Sigma) and applied in 25 μl aliquots to clipped dorsal skin. 48 hrs after FITC painting, inguinal lymph nodes were harvested with non-draining brachial lymph nodes for comparison. Lymph nodes were homogenised, passed through a 70 μm cell strainer, digested

in collagenase A (10 mg ml ml^{-1}) / DNAse I (1 mg ml ml^{-1}) (Roche, Indianapolis, IN), 2% FBS in PBS for 20 minutes, and cells analysed by flow cytometry. For the serum transfer model 200 μl of heat-inactivated WT or lupus serum was administered intraperitoneally to C57BL/6 mice 12 hours prior to FITC painting. For MMP-9 blocking studies, an anti-MMP-9 antibody (Ab-1, Calbiochem/ Merck Millipore, UK IM09L, clone 6.6B) was given at a dose of 4mg/kg intraperitoneally 12 hours prior to FITC painting and ova/ ova-ic administration. An isotype control antibody (mouse IgG_1, abcam, UK) was used at the same concentration as the anti-MMP-9 antibody.

Human serum for in vivo studies

Serum was obtained from six patients with SLE, three with low BILAG scores (2-9) and three with high BILAG scores (15-21) and three age and sex-matched healthy controls. Patient characteristics are detailed in Supplementary Table 1. Heat-inactivation was performed at 56 °C for 1 hour prior to administration. Samples were obtained with informed consent and approval of the Cambridge Local Research Ethical committee (reference 08/ H0308/176).

Image Analysis

Both *in vitro* and *in vivo* migration movies were processed using Imaris software (Version 6.2). The Snapshot tool was utilized to generate time-lapse movies (with 6-10 fps playback), still images, and track histories. To calculate forward protrusion alignment along the dominate CCL19 gradient, independent images from each group were selected, and the angle feature was applied to 20 cells per field to measure the angle between the leading edge and the dominant CCL19 gradient. To further characterize migration behavior, all DC migration data was analyzed using the ‘spots’ feature in Imaris. Specifically, X-Y coordinates for each cell tracked were exported to Microsoft Excel and plotted for spatial trajectories. Utilizing Imaris ‘spots’ feature, values for X displacement and track straightness were calculated for each individual track and plotted in Graphpad PRISM software. Migratory persistence was calculated by dividing displacement values by total path length. Percent distribution of velocities was calculated from the instantaneous velocities of each cell at each time-point, and binned over selected values. Average speed values were calculated over the entire movie. All chemotactic metrics were calculated in Excel.

Statistical analysis

Statistical analyses were performed using Graphpad PRISM software. A two-tailed Student’s t test was applied, unless otherwise indicated. Results are expressed as means and standard error of mean. All experiments were subject to at least three replicates per experimental parameter.

Supplementary Material

Refer to Web version on PubMed Central for supplementary material.

Europe PMC Funders Author Manuscripts

Acknowledgements

This work was supported by a Wellcome Trust Intermediate Fellowship (WT081020) to MRC, and by the NIHR Cambridge Biomedical Research Centre and the Intramural Research Program, NIAID, NIH. We thank J. Yoon for technical advice and M. Espeli for helpful discussions.

References

1. Banchereau J, Steinman RM. Dendritic cells and the control of immunity. Nature. 1998; 392:245–252. [PubMed: 9521319]
2. Steinman RM. Decisions about dendritic cells: past, present, and future. Annu Rev Immunol. 2012; 30:1–22. [PubMed: 22136168]
3. Krause RM, Dimmock NJ, Morens DM. Summary of antibody workshop: The Role of Humoral Immunity in the Treatment and Prevention of Emerging and Extant Infectious Diseases. J Infect Dis. 1997; 176:549–559. [PubMed: 9291299]
4. Joller N, Weber SS, Oxenius A. Antibody-Fc receptor interactions in protection against intracellular pathogens. Eur J Immunol. 2011; 41:889–897. [PubMed: 21413006]
5. Ravetch JV, Bolland S. IgG Fc receptors. Annu Rev Immunol. 2001; 19:275–290. [PubMed: 11244038]
6. Itano AA, et al. Distinct dendritic cell populations sequentially present antigen to CD4 T cells and stimulate different aspects of cell-mediated immunity. Immunity. 2003; 19:47–57. [PubMed: 12871638]
7. Hawiger D, et al. Dendritic cells induce peripheral T cell unresponsiveness under steady state conditions in vivo. J Exp Med. 2001; 194:769–779. [PubMed: 11560993]
8. Steinman RM, Hawiger D, Nussenzweig MC. Tolerogenic dendritic cells. Annu Rev Immunol. 2003; 21:685–711. [PubMed: 12615891]
9. Roake JA, et al. Dendritic cell loss from nonlymphoid tissues after systemic administration of lipopolysaccharide, tumor necrosis factor, and interleukin 1. J Exp Med. 1995; 181:2237–2247. [PubMed: 7760009]
10. Reis e Sousa C. Dendritic cells in a mature age. Nat Rev Immunol. 2006; 6:476–483. [PubMed: 16691244]
11. Boruchov AM, et al. Activating and inhibitory IgG Fc receptors on human DCs mediate opposing functions. J Clin Invest. 2005; 115:2914–2923. [PubMed: 16167082]
12. Dhodapkar KM, et al. Selective blockade of inhibitory Fcgamma receptor enables human dendritic cell maturation with IL-12p70 production and immunity to antibody-coated tumor cells. Proc Natl Acad Sci U S A. 2005; 102:2910–2915. [PubMed: 15703291]
13. Dhodapkar KM, et al. Selective blockade of the inhibitory Fcgamma receptor (FcgammaRIIB) in human dendritic cells and monocytes induces a type I interferon response program. J Exp Med. 2007; 204:1359–1369. [PubMed: 17502666]
14. Kalergis AM, Ravetch JV. Inducing tumor immunity through the selective engagement of activating Fcγ receptors on dendritic cells. J Exp Med. 2002; 195:1653–1659. [PubMed: 12070293]
15. van Montfoort N, et al. Fcgamma receptor IIb strongly regulates fcgamma receptor-facilitated T cell activation by dendritic cells. J Immunol. 2012; 189:92–101. [PubMed: 22649202]
16. Pricop L, et al. Differential modulation of stimulatory and inhibitory Fc gamma receptors on human monocytes by Th1 and Th2 cytokines. J Immunol. 2001; 166:531–537. [PubMed: 11123333]
17. Smith KGC, Clatworthy MR. FcγRIIB in autoimmunity and infection: evolutionary and therapeutic implications. Nat Rev Immunol. 2010; 10:328–343. [PubMed: 20414206]
18. Bolland S, Ravetch JV. Spontaneous autoimmune disease in Fc(gamma)RIIB-deficient mice results from strain-specific epistasis. Immunity. 2000; 13:277–285. [PubMed: 10981970]
19. Brownlie RJ, et al. Distinct cell-specific control of autoimmunity and infection by FcγRIIb. J Exp Med. 2008; 205:883–895. [PubMed: 18362174]

20. Boross P, et al. The inhibiting Fc receptor for IgG, FcγRIIB, is a modifier of autoimmune susceptibility. J Immunol. 2011; 187:1304–1313. [PubMed: 21724994]
21. Floto RA, et al. Loss of function of a lupus-associated FcγRIIb polymorphism through exclusion from lipid rafts. Nat Med. 2005; 11:1056–1058. [PubMed: 16170323]
22. Kono H, et al. FcγRIIB Ile232Thr transmembrane polymorphism associated with human systemic lupus erythematosus decreases affinity to lipid rafts and attenuates inhibitory effects on B cell receptor signaling. Hum Mol Genet. 2005; 14:2881–2892. [PubMed: 16115811]
23. Randolph GJ, Angeli V, Swartz MA. Dendritic-cell trafficking to lymph nodes through lymphatic vessels. Nat Rev Immunol. 2005; 5:617–628. [PubMed: 16056255]
24. Cyster JG. Chemokines and the homing of dendritic cells to the T cell areas of lymphoid organs. J Exp Med. 1999; 189:447–450. [PubMed: 9927506]
25. Forster R, et al. CCR7 coordinates the primary immune response by establishing functional microenvironments in secondary lymphoid organs. Cell. 1999; 99:23–33. [PubMed: 10520991]
26. Sallusto F, et al. Rapid and coordinated switch in chemokine receptor expression during dendritic cell maturation. Eur J Immunol. 1998; 28:2760–2769. [PubMed: 9754563]
27. Ratzinger G, et al. Matrix metalloproteinases 9 and 2 are necessary for the migration of Langerhans cells and dermal dendritic cells from human and murine skin. J Immunol. 2002; 168:4361–4371. [PubMed: 11970978]
28. Yen JH, Khayrullina T, Ganea D. PGE2-induced metalloproteinase-9 is essential for dendritic cell migration. Blood. 2008; 111:260–270. [PubMed: 17925490]
29. Lebre MC, Kalinski P, Das PK, Everts V. Inhibition of contact sensitizer-induced migration of human Langerhans cells by matrix metalloproteinase inhibitors. Arch Dermatol Res. 1999; 291:447–452. [PubMed: 10482016]
30. Kobayashi Y, Matsumoto M, Kotani M, Makino T. Possible involvement of matrix metalloproteinase-9 in Langerhans cell migration and maturation. J Immunol. 1999; 163:5989–5993. [PubMed: 10570286]
31. Ichiyasu H, et al. Matrix metalloproteinase-9-deficient dendritic cells have impaired migration through tracheal epithelial tight junctions. Am J Respir Cell Mol Biol. 2004; 30:761–770. [PubMed: 14656746]
32. Rahman A, Isenberg DA. Systemic lupus erythematosus. N Engl J Med. 2008; 358:929–939. [PubMed: 18305268]
33. Blanco P, Palucka AK, Gill M, Pascual V, Banchereau J. Induction of dendritic cell differentiation by IFN-alpha in systemic lupus erythematosus. Science. 2001; 294:1540–1543. [PubMed: 11711679]
34. Decker P, Kotter I, Klein R, Berner B, Rammensee HG. Monocyte-derived dendritic cells over-express CD86 in patients with systemic lupus erythematosus. Rheumatology (Oxford). 2006; 45:1087–1095. [PubMed: 16527880]
35. Ding D, Mehta H, McCune WJ, Kaplan MJ. Aberrant phenotype and function of myeloid dendritic cells in systemic lupus erythematosus. J Immunol. 2006; 177:5878–5889. [PubMed: 17056512]
36. Crispin JC, Vargas-Rojas MI, Monsivais-Urenda A, Alcocer-Varela J. Phenotype and function of dendritic cells of patients with systemic lupus erythematosus. Clin Immunol. 2012; 143:45–50. [PubMed: 22239954]
37. Willcocks LC, et al. A defunctioning polymorphism in FCGR2B is associated with protection against malaria but susceptibility to systemic lupus erythematosus. Proc Natl Acad Sci U S A. 2010; 107:7881–7885. [PubMed: 20385827]

Supplementary references

38. Schaefer BC, Schaefer ML, Kappler JW, Marrack P, Kedl RM. Observation of antigen-dependent CD8+ T-cell/ dendritic cell interactions in vivo. Cell Immunol. 2001; 214:110–122. [PubMed: 12088410]
39. Lindquist RL, et al. Visualizing dendritic cell networks in vivo. Nat Immunol. 2004; 5:1243–1250. [PubMed: 15543150]

40. Lammermann T, et al. Rapid leukocyte migration by integrin-independent flowing and squeezing. Nature. 2008; 453:51–55. [PubMed: 18451854]
41. Bowden ET, Coopman PJ, Mueller SC. Invadopodia: unique methods for measurement of extracellular matrix degradation in vitro. Methods Cell Biol. 2001; 63:613–627. [PubMed: 11060862]
42. Haessler U, Pisano M, Wu M, Swartz MA. Dendritic cell chemotaxis in 3D under defined chemokine gradients reveals differential response to ligands CCL21 and CCL19. Proc Natl Acad Sci U S A. 2011; 108:5614–5619. [PubMed: 21422278]
43. Tal O, et al. DC mobilization from the skin requires docking to immobilized CCL21 on lymphatic endothelium and intralymphatic crawling. J Exp Med. 2011; 208:2141–2153. [PubMed: 21930767]
44. Zinselmeyer BH, Lynch JN, Zhang X, Aoshi T, Miller MJ. Video-rate two-photon imaging of mouse footpad - a promising model for studying leukocyte recruitment dynamics during inflammation. Inflamm Res. 2008; 57:93–96. [PubMed: 18213448]
45. Robbiani DF, et al. The leukotriene C(4) transporter MRP1 regulates CCL19 (MIP-3beta, ELC)-dependent mobilization of dendritic cells to lymph nodes. Cell. 2000; 103:757–768. [PubMed: 11114332]

Europe PMC Funders Author Manuscripts

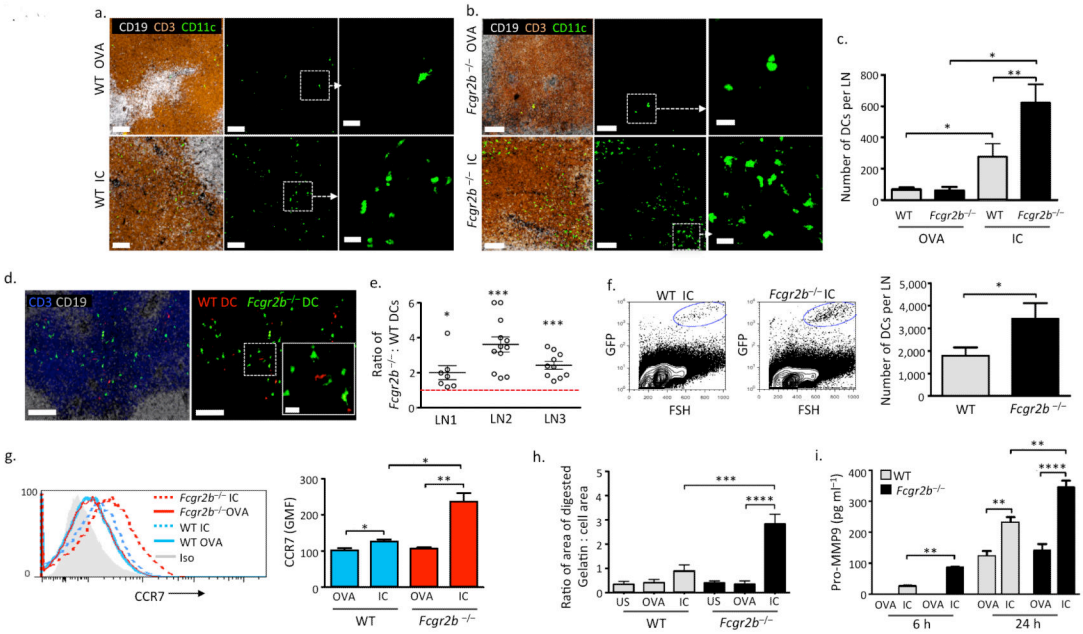

Figure 1. Immune complexes increase CCR7 expression, matrix metalloprotease production, and migration of murine bone marrow-derived DCs

Representative images of a draining lymph node 48 hours following subcutaneous transfer of bone marrow-derived DCs (BMDCs) (green) from WT (a) or *Fcgr2b*$^{-/-}$ (b) mice incubated with ovalbumin (OVA, upper panels) or IgG-opsonised ovalbumin (IC, lower panels) for 24 hours prior to transfer. B cell follicles shown in white (CD19) and T cells (CD3) in brown. Scale bars in left and middle panels = 80 μm. Right panels show high power image (scale bars = 20 μm). (c) Total number of WT and *Fcgr2b*$^{-/-}$ DCs per lymph node 48 hours following transfer, as enumerated from serial 50μm sections. Graph shows mean and standard error of mean (SEM). (d) Representative images of draining lymph node 48 hours following the transfer of BMDCs from WT (red) and *Fcgr2b*$^{-/-}$ (green) mice stimulated for 24 hours with IC. B cell stained with CD19 (white) and T cells with CD3 (blue). Scale bar = 100μm. Inset shows high power image of area outlined by white square (scale bar = 20μm). (e) Ratio of *Fcgr2b*$^{-/-}$ to WT IC-stimulated BMDCs in the paracortex of three lymph nodes (LN) 48 hours following subcutaneous transfer. Each point represents the ratio observed in a 50μm section. Bars show mean and standard error of mean. Red dashed line marks a ratio of 1 (value of equivalent DC migration). (f) Representative flow cytometric data from dissociated lymph nodes 48 hours following transfer of GFP+ mouse BMDCs. IC-stimulated WT BMDCs are shown in left panel and *Fcgr2b*−/− BMDCs in the middle panel. Right panel shows quantification of lymph node BMDCs by flow cytometry 48 hours following transfer (Mean and SEM from 7 lymph nodes from 4 mice in each group). (g) Representative histograms of CCR7 expression on WT (blue lines) and *Fcgr2b*−/− (red lines) BMDCs following 24 hours of incubation with OVA (solid lines) or IC (dotted lines) (left panel) and geometric mean fluorescence (GMF) of CCR7 staining in WT and *Fcgr2b*$^{-/-}$ BMDCs (right panel). (h) Gelatinase production as quantified by area of FITC-gelatin digested over 24 hours by DCs following FcγR cross-linking with IC. Graph shows mean and SEM values obtained from combined result of three separate experiments. (i)

Europe PMC Funders Author Manuscripts

MMP-9 levels in culture supernatants obtained from WT and *Fcgr2b*$^{-/-}$ BMDCs 6 and 24 hours following incubation with OVA or IC. Graph shows mean and SEM of triplicates from representative experiment of three repeats. *P* values calculated using a Student's t test (two-tailed). * = $P \leq 0.05$, ** = $P \leq 0.01$, *** = $P \leq 0.001$, **** = $P \leq 0.0001$.

Europe PMC Funders Author Manuscripts

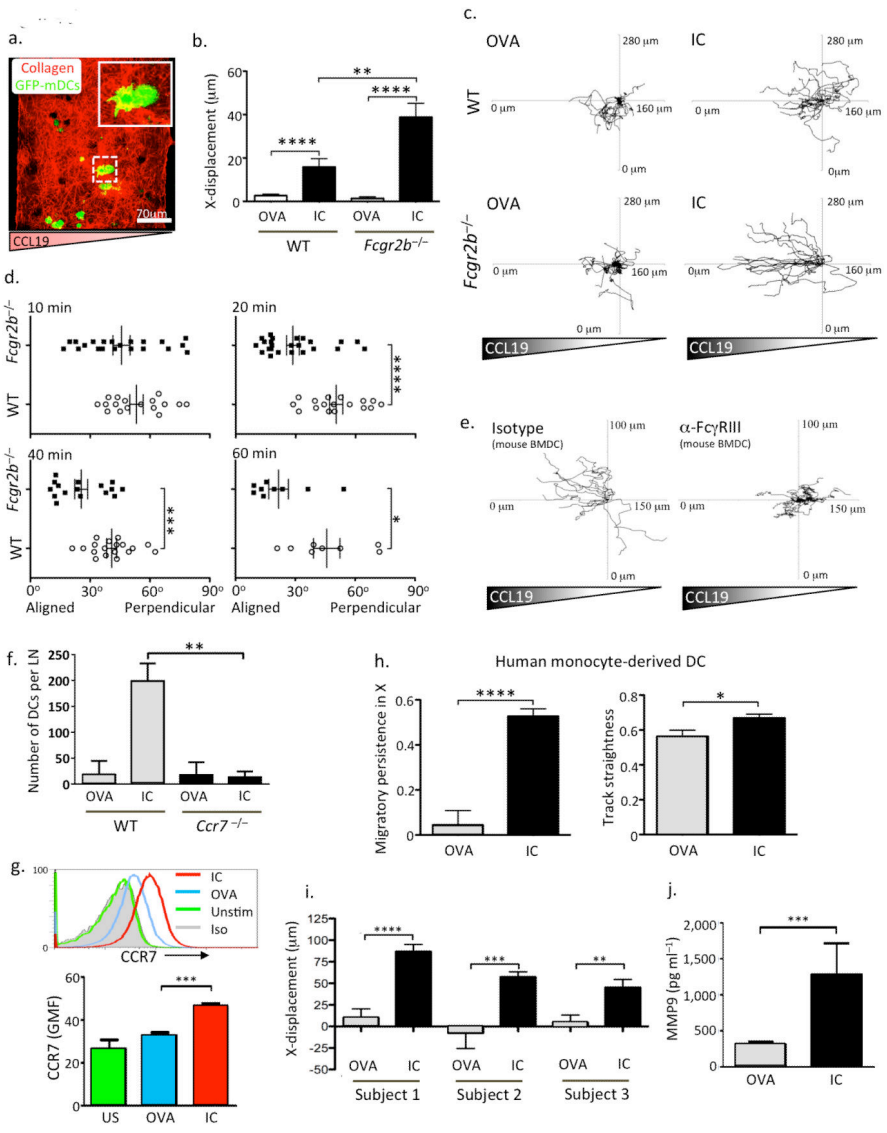

Figure 2. Immune complex FcγR engagement promotes chemokine-directed mouse and human DC migration *in vitro*

(a) Representative image of WT bone marrow-derived DCs ((BMDCs), GFP, green) embedded in a collagen matrix (red) prior to the application of a CCL19 gradient. (b) X-displacement of WT and *Fcgr2b*$^{-/-}$ BMDCs incubated with ovalbumin (OVA) or IgG-opsonised ovalbumin (IC) for 24 hours prior to incorporation within a collagen matrix and subsequent exposure to a CCL19 gradient. Graphs show mean and SEM of values obtained from one collagen gel, representative of at least three experimental replicates. (c) Representative migration tracks in a CCL19 gradient of WT (upper panels) and *Fcgr2b*$^{-/-}$ (lower panels) BMDCs incubated with OVA (left panels) or IC (right panels) for 24 hours prior to suspension in the collagen matrix. (d) Angle of leading protrusion relative to chemokine gradient of WT (open circles) and *Fcgr2b*$^{-/-}$ (filled squares) BMDCs suspended in a collagen matrix at 10, 20, 40, and 60 minutes following application of CCL19 gradient. Angles closer to 0° indicate cell polarization parallel to the gradient. (e) Representative

Europe PMC Funders Author Manuscripts

migration tracks in a CCL19 gradient of BMDCs incubated with IC, either in the presence of an FcγRIII blocking antibody (right panel) or an isotype control antibody (left panel). (f) Quantification of number of WT and *Ccr7*$^{-/-}$ DCs within draining lymph nodes 48 hours following subcutaneous transfer. Mean and SEM from 6 lymph nodes from 3 mice in each group shown. (g) CCR7 expression on human monocyte-derived DCs incubated with OVA (blue line) or IC (red line) for 24 hours. Representative histograms are shown in the upper panel and GMF and SEM of triplicates from one of three replicates shown in the lower panel. (h) Migratory persistence in X (left panel) and track straightness (right panel) of human monocyte-derived DCs in a human CCL19 gradient following incubated with OVA or IC for 24 hours prior. Values represent the mean and SEM from cells migrating in at least three collagen gels per subject and from three healthy subjects. (i) X-displacement of human monocyte-derived DCs from 3 subjects following application of a CCL19 gradient. Values represent the mean and SEM. (j) MMP-9 levels in culture supernatants obtained from human monocyte-derived DCs isolated from 3 healthy subjects. Values represent the mean and SEM. In (c) and (e), tracks are derived from a single collagen gel and representative of three similar experiments. *P* values calculated using a Students t test (two-tailed). * = $P \leq 0.05$, ** = $P \leq 0.01$, *** = $P \leq 0.001$, **** = $P \leq 0.0001$.

Europe PMC Funders Author Manuscripts

Europe PMC Funders Author Manuscripts

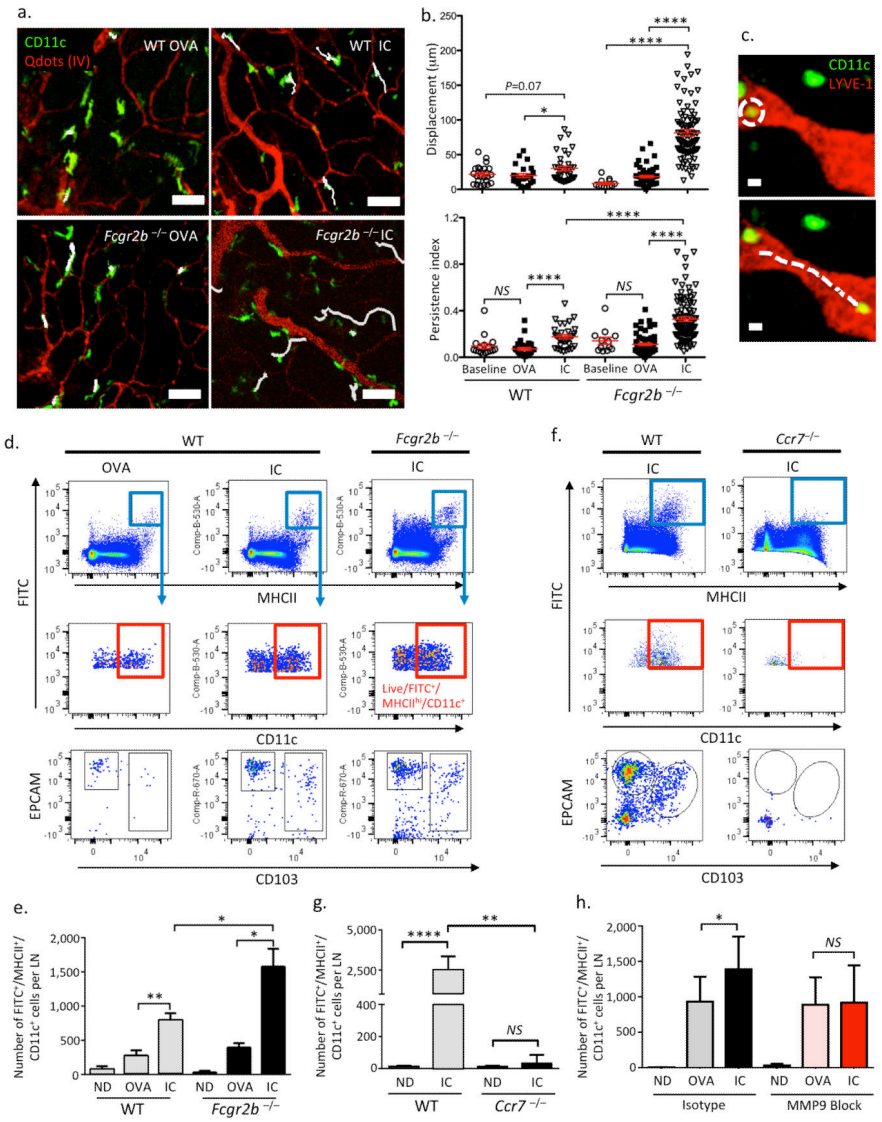

Figure 3. Immune complexes stimulate CCR7-dependent dermal dendritic cell migration to lymph nodes *in vivo*

(a) Footpad dermal DCs (green) were imaged by two-photon microscopy in WT CD11cEYFP (upper panels) and *Fcgr2b*$^{-/-}$ CD11cEYFP mice (lower panels), 16 hours following the administration of ovalbumin (OVA) or IgG-opsonised ovalbumin (IC) subcutaneously to the footpad. Blood vessels are shown in red (Qdots IV) and cell tracks over an 80 minute period shown in white. Scale bars = 50 μm. Quantification of displacement and persistence index for dermal DCs from three mice in each group is shown in (b). (c) Sequential images obtained by intravital two-photon microscopy of the footpad 16 hours after IC administration. Movement of a dermal DC (green) tracked (white broken line) through a dermal lymphatic vessel (LYVE-1, red). Scale bars = 10 μm. Representative flow cytometric plots and quantification of live/FITC^{+}/MHCII^{high}/CD11c^{+} cells in draining lymph nodes in WT and *Fcgr2b*$^{-/-}$ mice (d and e) and WT and *Ccr7*$^{-/-}$ mice (f and g) 48 hours after application of FITC to skin followed by intradermal administration of OVA or

IC as indicated. Mean and SEM from 4 mice in each group shown. *P* values calculated using a Students t test (two-tailed). (h) Quantification of live/FITC^{+}/MHCII^{high}/CD11c^{+} cells present in draining lymph nodes of WT mice treated with MMP-9 blocking antibody or isotype control prior to application of FITC to skin with intradermal administration of OVA or IC. Mean and SEM from 4 mice in each group shown. *P* values calculated using a paired t test to compare lymph nodes draining skin treated with OVA (left inguinal) and IC (right inguinal) or non-draining lymph nodes (brachial) from the same mouse. * = $P \leq 0.05$, ** = $P \leq 0.01$, *** = $P \leq 0.001$, **** = $P \leq 0.0001$.

Europe PMC Funders Author Manuscripts

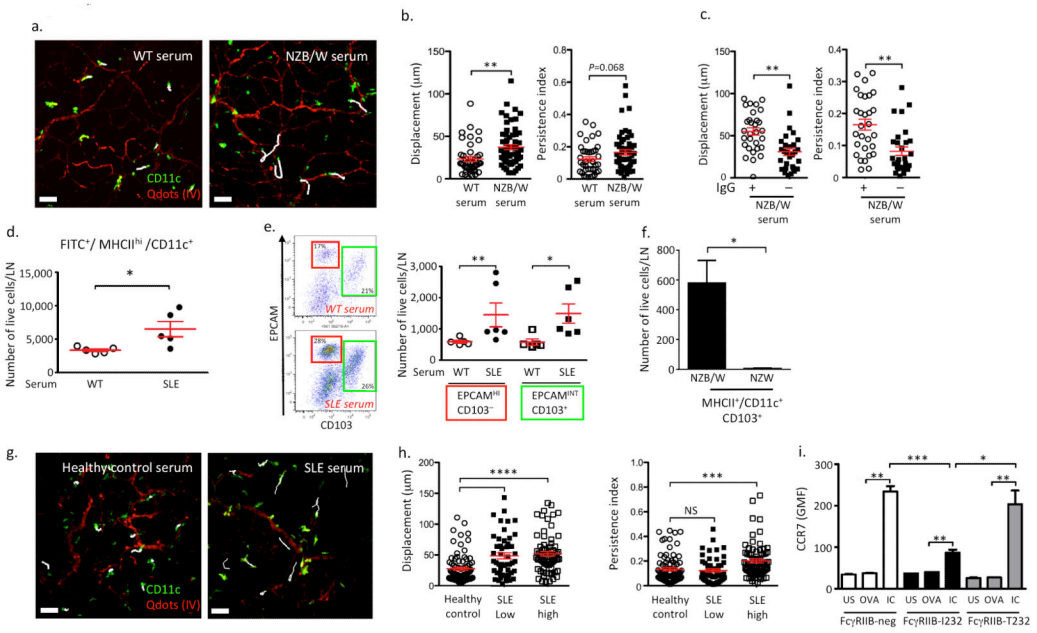

Figure 4. Murine and human lupus sera stimulate dermal dendritic cell migration to lymph nodes *in vivo*

(a) Cell tracks (white) of footpad dermal DCs (green) 16 hours following the administration of heat-inactivated, aged WT mouse serum, or serum obtained from autoimmune NZB/W F1 mice. Blood vessels shown in red (Qdots IV) and cell tracks over an 80 minute period in white. Scale bar = 50μm. Quantification of displacement and persistence index of dermal DCs from three mice in each group is shown in (b). (c) Quantification of displacement and persistence index of footpad dermal DCs in CD11cEYFP mice 16 hours following the administration of heat-inactivated, NZB/W F1 mouse serum containing IgG (IgG+) or an aliquot depleted of IgG (IgG-). (d) Number of live/FITC^{+}/MHCII^{high}/CD11c^{+} cells per draining lymph node in WT mice and (e) Representative flow cytometric plots (left panel) and quantification (right panel) of FITC^{+}/MHCII^{high}/CD11c^{+}/EPCAM^{+} (Langerhans cells) and CD11c^{+}/CD103^{+} (dermal DCs) in draining lymph nodes 48 hours after application of FITC to skin in mice given heat-inactivated WT (open circles) or SLE (black circles) serum intraperitoneally 12 hours previously. Each circle in d and e represents quantification from a single lymph node. (f) Number of CD11c^{+}/MHCII^{high}/CD103^{+} cells in renal lymph nodes of aged NZM mice with lupus nephritis and aged-match NZW controls. Graphs show mean and SEM of lymph nodes taken from four mice. (g) Representative cell tracks (white) of footpad dermal DCs (green) and (h) Quantification of displacement and persistence index of dermal DCs in WT mice 16 hours following the administration of heat-inactivated serum obtained from healthy controls or from patients with SLE. Scale bar in g = 50 μm. Graphs show values from mice treated with three healthy control sera (open circles) or from three SLE patients with low disease activity (BILAG scores 2-9, filled squares, ‘SLE low’) or three SLE patients with high disease activity (BILAG scores 15-21, open squares, ‘SLE high’). (i) CCR7 expression on WT U937 cells or those stably expressing FcγRIIB-I232 or FcγRIIB-T232 24 hours following incubation with OVA or IC. Graph shows mean and SEM of duplicates from one of three experiments. In (b), (c), and (h) each point represents a

Europe PMC Funders Author Manuscripts

single dermal DC, and the bar shows the mean value. *P* values calculated using a Students t test (two-tailed). * = $P \leq 0.05$, ** = $P \leq 0.01$, *** = $P \leq 0.001$, **** = $P \leq 0.0001$.

Europe PMC Funders Author Manuscripts